Computers and Geotechnics 97 (2018) 103–110

Contents lists available at ScienceDirect

Computers and Geotechnics

journal homepage: www.elsevier.com/locate/compgeo

Technical Communication

Upper-bound stability analysis of dual unlined horseshoe-shaped tunnels subjected to gravity

Jian Zhang[a], Tugen Feng[a], Junsheng Yang[b,*], Feng Yang[b], Yufeng Gao[a]

[a] College of Civil and Transportation Engineering, Hohai University, Nanjing, Jiangsu 210098, China
[b] School of Civil Engineering, Central South University, Changsha, Hunan 410075, China

ARTICLE INFO

Keywords:
Horseshoe-shaped tunnel
Stability
Collapse mechanism
Upper-bound finite element method
Adaptive meshing

ABSTRACT

This study investigates the stability of dual horseshoe-shaped tunnels in cohesive-frictional soils subjected to gravity using an upper-bound finite element method combined with a plastic-dissipation-based mesh adaptive strategy. The results are presented in the form of dimensionless stability numbers, which decrease with C/D and increase with ϕ. The results indicate that the interaction between dual horseshoe-shaped tunnels disappears when their dimensionless center-to-center distance S/D lies approximately in any of the following ranges for C/D: (i) 3.5–4.5 for $C/D = 1$, (ii) 3.5–6.5 for $C/D = 2$, (iii) 3.5–9 for $C/D = 3$, (iv) 4–11 for $C/D = 4$, and (v) 4–13.5 for $C/D = 5$.

1. Introduction

Horseshoe-shaped tunnels were initially constructed for applications such as mining, highway tunnels, and railway tunnels. In modern times, they have been widely used in city infrastructure and transportation systems within large cities. In general, given economic and practical concerns, as well as geological conditions, the use of multiple tunnels has become a viable option which results in the construction of tunnels located side by side. However, for relatively low center-to-center distances, there are non-negligible interactions between these dual tunnels. The stability of these tunnels is worse than that of single tunnels, and their collapse mechanisms also differ from that of single tunnels. Consequently, an accurate assessment of the interactions between dual tunnels is required.

Numerical methods [1–7] and model testing [8–11] have been used to analyze the behavior of dual tunnels considering the ground deformation that occurs during tunnel construction. However, only a few studies have focused on the stability of dual tunnels. Limit analysis methods have proven to be an effective means of determining the stability of dual tunnels [12–19], as they make it easy to perform the large amount of calculations associated with collapse mechanisms. Osman [12] evaluated the undrained stability of unlined dual tunnels by superimposing the continuous plastic deformation mechanism from each tunnel. Sahoo and Kumar [13] investigated the variation of stability number and nodal velocity pattern for dual unlined circular tunnels under the influence of gravity. Yamamoto et al. [14,15] presented the upper- and lower-bound solutions for dual unsupported tunnels affected by surcharge loads. Subsequently, Wilson et al. [16,17] obtained upper- and lower-bound estimates for the undrained stability of dual tunnels. Yang et al. [18] and Yang et al. [19] analyzed the collapse mechanisms of dual tunnels subjected to gravity.

While previous studies mainly analyzed the stability of dual circular tunnels and dual square tunnels, in this paper, the upper-bound finite element method (UBFEM) is used to investigate the stability of dual horseshoe-shaped tunnels in soils subjected to gravity. For tunnels in cohesive-frictional soils, it is difficult to obtain a good failure mechanism using relatively few constant strain elements; therefore, higher-order triangle elements (six-nodal triangle elements) in combination with a plastic-dissipation-based mesh adaptive strategy are adopted to improve the accuracy of computations. The stability of dual horseshoe-shaped tunnels is determined using a dimensionless stability number that is affected by the dimensionless center-to-center distance S/D, dimensionless depth C/D, and soil properties. A refined collapse mechanism that can explicitly reflect slip lines is also presented. Finally, the results are compared with those previously reported in the literature.

2. Problem description

In this study, it is assumed that dual unlined tunnels with horseshoe-shaped cross-sectional profiles are sufficiently long relative to their dimensions that they can be simplified using the plane strain analysis model. Because a horseshoe-shaped tunnel has complex curves and the tunnel geometry has no strict definition, in this paper, the cross-section

* Corresponding author.
E-mail address: jsyang@csu.edu.cn (J. Yang).

https://doi.org/10.1016/j.compgeo.2018.01.006
Received 12 August 2017; Received in revised form 18 December 2017; Accepted 12 January 2018
0266-352X/ © 2018 Elsevier Ltd. All rights reserved.

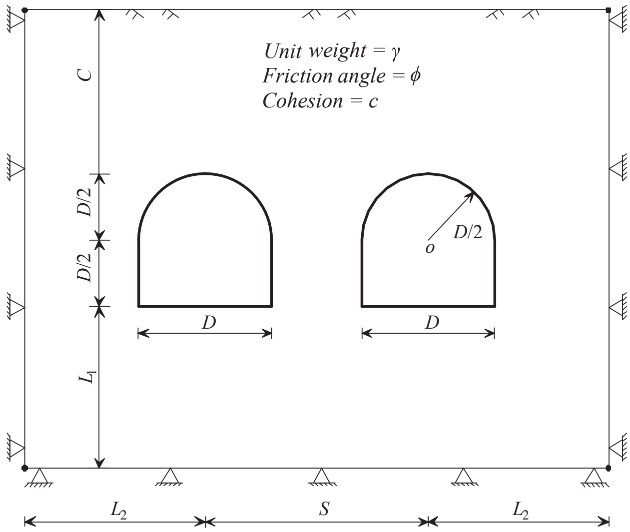

Fig. 1. Analysis model for dual horseshoe-shaped tunnels.

of the horseshoe-shaped tunnel is typified as consisting of a semi-circular roof and a flat floor, as shown in Fig. 1. Each tunnel has a semi-circular roof with radius $D/2$ and a flat floor with height $D/2$ and span D. Dual tunnels are aligned horizontally with a center-to-center distance S and located at a depth C below the surface of the ground. The soil mass is either modeled as a Tresca material (fully cohesive soils) or a Mohr-Coulomb material (cohesive-frictional soils) with cohesion c, internal friction angle ϕ, and unit weight γ. No surcharge loads are assumed to act on the ground surface, and no lining is placed along the tunnel boundary. Tunnel collapse is driven only by the action of gravity, and the stability of dual horseshoe-shaped tunnels can be conveniently described in terms of a dimensionless stability number ($N = \gamma D/c$), which is influenced by C/D, ϕ, and S/D.

Fig. 2 shows the initial finite element meshes for the case with $C/D = 2$ and $S/D = 3$, and similar mesh patterns are applied in the other cases. Only the right half of the problem domain is necessary to investigate this issue because of its symmetry. Note that n_1 is the total number of nodes, and n_e is the total number of elements in the domain. As seen in Fig. 2, the boundary dimensions (L_1 and L_2) are $2D$ and $5D$, respectively, and these values increase with tunnel depth. The problem domain is discretized with six-nodal triangular elements, and the element size gradually decreases toward the periphery of the tunnels. Both the horizontal and vertical velocity components are specified as zero along the boundaries QM and MN, and the horizontal velocity component equals zero along boundary PQ (i.e., the symmetric boundary). No velocity constraints are applied on the ground surface and along the tunnel boundary.

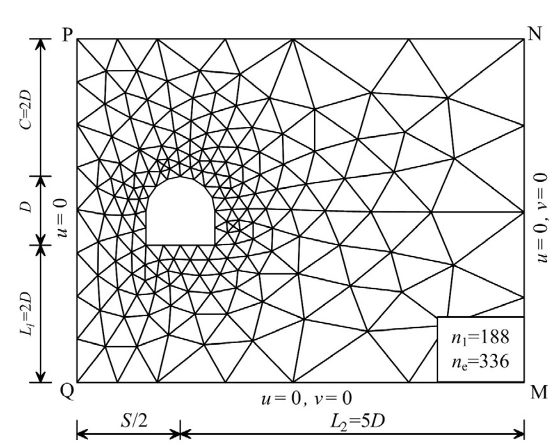

Fig. 2. Initial finite element meshes for the case with $C/D = 2$ and $S/D = 3$.

3. UBFEM with a mesh adaptive strategy

Inspired by the ideas of compensating for the low order of three-nodal elements presented by some researchers [20–23], the UBFEM with higher-order elements (six-nodal elements) is used to analyze the stability of dual unlined horseshoe-shaped tunnels. In contrast to second-order cone programming [22], in this paper, upper bound limit analysis is formulated as a linear programming problem following the Mohr-Coulomb yield criterion. This requires linearization of the failure criterion with the polygon that is circumscribed to the yield criterion. As the strain tensor varies linearly within the six-nodal element, it is necessary to enforce the flow rule at the three vertices of each element. To determine the stability of dual horseshoe-shaped tunnels subjected to gravity, an upper bound on critical weight ($\gamma_{\min}$) can be obtained by minimizing the internal power dissipation with respect to the velocity boundary conditions, flow rule and compatibility requirements.

The linear programming model takes the following form:

$$\text{Minimize } \gamma_{\min} = \sum_{m=1}^{n_e} P_p^m \tag{1}$$

Subject to

$$\begin{cases} \frac{\partial u_{(m)}}{\partial x}(x = x_i, y = y_i) = \dot{\varepsilon}_{i,x}^m = \sum_{k=1}^{p} \dot{\lambda}_{i,k}^m \frac{\partial F_k^m}{\partial \sigma_x^m} = \sum_{k=1}^{p} \dot{\lambda}_{i,k}^m A_k^m & \text{(a)} \\ \frac{\partial v_{(m)}}{\partial y}(x = x_i, y = y_i) = \dot{\varepsilon}_{i,y}^m = \sum_{k=1}^{p} \dot{\lambda}_{i,k}^m \frac{\partial F_k^m}{\partial \sigma_y^m} = \sum_{k=1}^{p} \dot{\lambda}_{i,k}^m B_k^m & \text{(b)} \\ \left(\frac{\partial u_{(m)}}{\partial y} + \frac{\partial v_{(m)}}{\partial x}\right)(x = x_i, y = y_i) = \dot{\gamma}_{i,xy}^m = \sum_{k=1}^{p} \dot{\lambda}_{i,k}^m \frac{\partial F_k^m}{\partial \tau_{xy}^m} = \sum_{k=1}^{p} \dot{\lambda}_{i,k}^m C_k^m & \text{(c)} \\ \dot{\lambda}_{i,k}^m \geqslant 0,\ i = 1,2,3;\ m = 1,2,\ldots n_e & \text{(d)} \\ u_{b,j} = 0\ (j = 1,\ldots,n_{m1}) & \text{(e)} \\ u_{b,j} = 0, v_{b,j} = 0\ (j = 1,\ldots,n_{m2}) & \text{(f)} \\ u_{b,j} = 0, v_{b,j} = 0\ (j = 1,\ldots,n_{m3}) & \text{(g)} \\ \sum_{m=1}^{n_e} \int_{A_m} v_{(m)} dA = 1 & \text{(h)} \end{cases} \tag{2}$$

where $\sum_{m=1}^{n_e} P_p^m = \sum_{m=1}^{n_e} \int_{A_m} (\sigma_x^m \dot{\varepsilon}_{i,x}^m + \sigma_y^m \dot{\varepsilon}_{i,y}^m + \tau_{xy}^m \dot{\gamma}_{i,xy}^m) dA = 2/3c\cos\phi \sum_{m=1}^{n_e} A_m \sum_{i=1}^{3} \sum_{k=1}^{p} \dot{\lambda}_{i,k}^m$ defines the power dissipated by all the elements, A_m represents the area of the mth element, and p is the total number of sides of the polygon that is used to linearize the failure criterion. Eqs. (2a)-(2c) define the flow rule within elements, ($u_{(m)}$,$v_{(m)}$) are the velocities of an arbitrary point for the mth element in the horizontal- and vertical-directions, and (x_i,y_i) define the nodal coordinates for the ith vertex. Given the lack of velocity discontinuities, each node is shared by the adjacent elements, and the velocities of the ith vertex for adjacent elements remain the same. ($\dot{\varepsilon}_{i,x}^m$,$\dot{\varepsilon}_{i,y}^m$,$\dot{\gamma}_{i,xy}^m$) define the strain rates of the ith vertex in the mth element, F_k^m is the function of the kth side of the yield polygon, (σ_x^m,σ_y^m,τ_{xy}^m) define the stresses for the mth element, (A_k^m,B_k^m,C_k^m) are parameters corresponding to the polygon yield criterion for the ith vertex in the mth element, and $\dot{\lambda}_{i,k}^m$ defines the non-negative plastic multiplier rate for the ith vertex. Eqs. (2e)-(2g) define the constraints of the velocity boundaries, where (n_{m1}, n_{m2}, n_{m3}) are the total number of nodes at boundaries PQ, QM, and MN, and ($u_{b,j}$,$v_{b,j}$) define the velocities of nodes along the boundaries in the horizontal- and vertical-directions. Eq. (2h) is imposed to initiate tunnel collapse.

The explanations of the objective function and constraints are similar to those given by Sloan and Kleeman [24] and Makrodimopoulos and Martin [22].

To obtain upper-bound solutions with good accuracy and plastic regions with strong identifiability, a plastic-dissipation-based mesh

Download English Version:

https://daneshyari.com/en/article/6709724

Download Persian Version:

https://daneshyari.com/article/6709724

Daneshyari.com